Inertial Sensor-Assisted High-Coverage Visible Light Positioning Algorithm

Fugui He, Chengyang Li, Chensitian Zhang, Yao Nie, Huan Wu, Xianglin Fan, Yang Yang

***Abstract*—Existing visible light positioning (VLP) algorithms typically require multiple LEDs to achieve high-precision positioning. However, in practice, the number of available LEDs is influenced by various factors such as the layout of LEDs and the field-of-view of the receiver, and these factors can significantly affect the coverage of a VLP algorithm. To address this issue, this paper proposes an inertial sensor-assisted single view geometry (ISA-SVG) algorithm, which can achieve accurate positioning as little as one LED. In particular, we first establish the projection transformation model between the actual point and its projection on the image plane. Then, a pose fusion model that effectively fuses the inertial sensor information and VLP information is established. Finally, the position of the receiver based on the pose fusion model is estimated. IAS-SVG significantly improves the usability and coverage performance of visible light positioning algorithms. Simulation results show that the coverage rate of the ISA-SVG algorithm is over 95%. Experimental results show that the proposed method can achieve an average positioning error as low as 4.70 cm.**

***Index Terms*—visible light positioning, indoor positioning, visual information, inertial sensor.**

I. Introduction

Accurate indoor positioning has attracted increasing attention due to extensive applications in emergent applications like the Internet of Things (IoT) [1], extended reality [2], and smart environments [3]. To satisfy different service requirements and applications, several popular wireless positioning technologies have been proposed including ultra-wide bandwidth (UWB) [4], WiFi [5], and Bluetooth [6]. Although all these positioning technologies have shown their advantages in a certain aspect, till now, they still face challenges on the trade-off between the cost and the accuracy [7].

Under this background, visible light positioning (VLP) has been extensively studied [8], which is promising to achieve accurate and low-cost positioning simultaneously. In particular, VLP reuses existing light-emitting diodes (LEDs) as transmitters and light sensors like the cameras on smartphones and photodiodes (PDs) as receivers, and thus VLP is a low-cost technology. Moreover, considering the directional propagation feature of the light, VLP is accurate in nature due to the limited inter-interference and relatively stable channel state information.

There is a plethora of prior art on VLP, and this work divides the existing VLP studies into three types, i.e. PD-based [9], camera-based [10] and fusion-based [11] VLP systems. In particular, for PD-based VLP, PD can easily estimate the signal strength of the received visible light signals. Therefore, PD-based VLP algorithms can achieve proximity, fingerprinting [12] and RSS/RSSR algorithms [13]. In contrast, for camera-based VLP systems, the camera captures the information of LEDs via rolling shutter effects. The camera-based VLPs have several unique features compared to PD-based systems, such as a larger field of view and spatial separation capability of light [7]. Moreover, the above PD- and camera-based studies typically require multiple LEDs to achieve precise positioning, which may not be practical in scenarios where LEDs are deployed sparsely.

To solve the above challenges, fusion-based VLP has been studied, which aims to combine the advantages of multiple sensors to achieve accurate and robust VLP. For instance, the authors in [14] combined a motion sensor and a camera to achieve indoor positioning. However, this method [14] requires at least three LEDs for accurate positioning, and thus its coverage is limited. Here, the coverage refers to the proportion of indoor locatable area to the entire positioning area. For the algorithm [14], the areas with less than three receivable LEDs are considered as unlocatable areas. To enhance the coverage, the authors in [15] proposed to use the accelerometer and geomagnetic field sensor to achieve single-LED VLP. However, this method requires a certain type of LED (i.e. circular LED), and substantial errors occur in the estimation of the circular LED diameter especially when the receiver is tilted at a large angle. This will lead to positioning accuracy degradation. To reduce the estimation error, the authors [16] proposed to use a value between the elliptical major axis and the real projection to approximate the

This research was funded by the National Natural Science Foundation of China under Grant No. 61702375, the Natural Science Research Project of Colleges and Universities in Anhui Province under Grant No. 2022AH051782 and WXZR202220, the Natural Science Foundation of Anhui Province under Grant 2108085QA10,the open fund of Information Materials and Intelligent Sensing Laboratory of Anhui Province under Grant No. IMIS202010, the excellent young talents support program in universities of Anhui Province under Grant No. 2022AH020091, the outstanding Youth Talent Support Program in Universities of Anhui Province under Grant No. gxyqZD2021128, the major Project of Anhui education department under Grant KJ2021ZD0116, Research Foundation of high-level talent of West Anhui University under Grant No.WGKQ202001006, the project of Young Core Teacher in Higher Education of Anhui under Grant No.gxyq2019070.

Fugui He is with School of Electronic and Information Engineering, West Anhui University, Lu'an, Anhui 237012, China and Information Materials and Intelligent Sensing Laboratory of Anhui Province, Anhui University, Hefei, Anhui 230039, China(e-mail: fuguihe@wxc.edu.cn,).

Chengyang Li is with Bestpay Co. Ltd, Xian 100031, China (e-mail: lichengyang@bestpay.com.cn).

Chensitian Zhang is with International School of Beijing University of Posts and Telecommunications, Beijing 100876, China (e-mail: zcst@bupt.edu.cn,).

Yao Nie, Huan Wu, Xianglin Fan are with School of Electronic and Information Engineering, West Anhui University, Lu'an, Anhui 237012, China (e-mail: nieyao@wxc.edu.cn, wuhuan@wxc.edu.cn, 276789590@qq.com).

Yang Yang is with School of Information and Communication Engineering, Beijing University of Posts and Telecommunications, Beijing 100876, China (e-mail: yangyang01@bupt.edu.cn,).

exact projection, thereby reducing the approximation error and improving positioning accuracy. However, the approximation error still exists. Moreover, the authors in [17] presented an enhanced positioning system that integrates single-lamp VLP with inertial measurement units (IMUs). By employing a novel multi-frame fusion method for LED-ID decoding, the system significantly reduces accumulated errors, achieving real-time and accurate positioning with a decoding accuracy of 98.5% and an average localization accuracy within 0.5 m. However, the algorithm relies on the vertical reception assumption of VLP signals. That means the tilt or obstruction of cameras can lead to trajectory drift. Overall, the existing fusion-based VLP algorithm still has certain practical limitations on the type of used LEDs, the number of receviable LEDs, etc. Therefore, a high-coverage, practical VLP algorithm still needs further investigation.

The main contribution of this work is a fusion-based VLP algorithm, i.e. inertial sensor-assisted single view geometry (ISA-SVG) algorithm that can achieve accurate positioning using only one LED without any receiver tilt limitation. In particular, we first establish the projection transformation model between the actual point and its projection on the image plane. Then, a novel fusion model between the attitude information and the visible light information is established. Based on the fused information, the position of the receiver is finally estimated. Since ISA-SVG does not rely on any geometry information of LEDs, ISA-SVG is applicable to any type of LEDs. To verify the feasibility of the proposed ISA-SVG algorithm, we establish a prototype based on a smartphone and several commercial-off-the-shelf LEDs. Simulation results verify that ISA-SVG can cover more than 95% indoor areas. Experimental results show that the proposed method can achieve an average positioning error as low as 4.70 cm.

The rest of the paper is organized as follows. In section II, we introduce the system model. Sections III and IV introduce the proposed ISA-ASG and its implementation, respectively. Next, Section V illustrates the simulation and experimental results. Finally, Section VI concludes this paper.

II. System Model

Fig. 1 illustrates the considered system model, where K LEDs are installed in the ceiling as transmitters, and a user holds a smartphone to locate its own position. Each LED constantly broadcasts position information, which consists of the identification (ID) and the world coordinate of the LED. The receiver is a smartphone, which is typically equipped with image sensors and inertial sensors. The image sensor is used to receive the visible light signal, while the inertial sensor is used to obtain the Euler angles including pitch, roll, and azimuth angles of the receiver. The target of this work is to jointly utilize the information from the image and inertial sensors to achieve high coverage and accurate positioning. Let $\mathbf{s}_i^{\mathrm{w}} = (x_i^{\mathrm{w}}, y_i^{\mathrm{w}}, z_i^{\mathrm{w}})^{\mathrm{T}} (i \in \{1, 2, \cdots, K\})$ be the world coordinates of the ith LED, and $\mathbf{r}^{\mathrm{w}} = (x_r^{\mathrm{w}}, y_r^{\mathrm{w}}, z_r^{\mathrm{w}})^{\mathrm{T}}$ be the world coordinates of the receiver to be determined.

In the system model, five coordinate systems are constructed to accurately analyze the positional relations between the LED and the camera. In particular, the four coordinate systems are i) 3D world coordinate system (WCS) $o^w - x^w y^w z^w$, ii) 3D camera coordinate system (CCS) $o^c - x^c y^c z^c$, iii) 2D image coordinate system (ICS)$o^i - x^i y^i$, and iv) 2D-pixel coordinate system (PCS) $o^p - u^p v^p$. Additionally, we further construct an auxiliary coordinate system (ACS) $o^{\mathrm{a}} - x^{\mathrm{a}} y^{\mathrm{a}} z^{\mathrm{a}}$ to represent the Euler angle information from the inertial sensor.

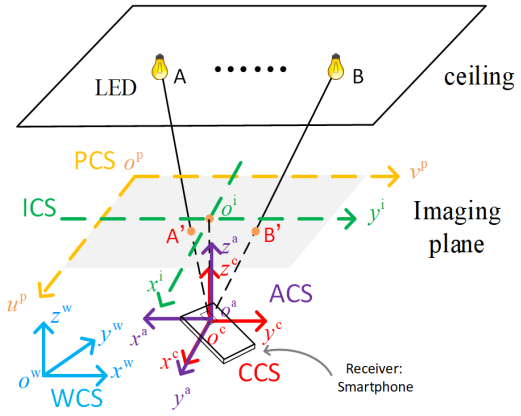

Fig. 1. System Model.

As shown in Fig. 1, in PCS, ICS, and CCS, the axes u^p, x^i and x^c are parallel to each other. Similarly, v^p, y^i and y^c are also parallel. In WCS, the z^w-axis is upward and vertical to the ground, and the x^w-axis and y^w-axis are parallel to the walls. Additionally, point o^p is located at the top left corner of the imaging plane, point o^i is at the center of the imaging plane, known as the principal point, with pixel coordinates $(u_0^{\mathrm{p}}, v_0^{\mathrm{p}})^{\mathrm{T}}$, where o^c is the optical center of the image sensor and is situated on the optical axis. Since the focal length f is the distance between points o^c and o^i, and the z-axis coordinates of all projection points on the image plane CCS are equal to f. Furthermore, the projection of the ith LED on the imaging plane lies on the same line with o^c. For any point P in a finite space, its corresponding coordinates in the WCS and CCS can be denoted as P^{w} and P^{c} respectively. The transformation from CCS to WCS can be represented as

$$\mathbf{P}^{\mathrm{w}} = \mathbf{R}_{\mathrm{c}}^{\mathrm{w}} \mathbf{P}^{\mathrm{c}} + \mathbf{T}_0 \tag{1}$$

where $\mathbf{R}_{\mathrm{c}}^{\mathrm{w}}$ is the rotation matrix and $\mathbf{T}_0$ is the translation vector. Note that $\mathbf{T}_0$ also represents the position coordinates of the camera in WCS, i.e. the positioning target. In a general positioning model, both the rotation matrix $\mathbf{R}_{\mathrm{c}}^{\mathrm{w}}$ and the translation vector $\mathbf{T}_0$ need to be calculated.

In addition, due to the imaging principle of the camera, there is a one-to-one correspondence between points on the image and corresponding points on the actual object. This is reflected in the CCS and ICS by the same geometric similarity relationship in the point coordinates of the "object-image" point pairs. This similarity property is reflected in the imaging process shown in Fig. 1. In particular, the relationship between

the coordinates of points in ICS and CCS can be easily represented as follows

$$\begin{cases} x/X^{\mathrm{c}} = f_0/Z^{\mathrm{c}} \\ y/Y^{\mathrm{c}} = f_0/Z^{\mathrm{c}} \end{cases} \tag{2}$$

where (x, y) represents the coordinates of a point in ICS and $(X^{\mathrm{c}}, Y^{\mathrm{c}}, Z^{\mathrm{c}})$ represents the coordinates of the point in the CCS, and f_0 is the focal length of the camera. From (2), it can be observed that there is a linear relationship between the horizontal and vertical coordinates and the height coordinates in the CCS. Moreover, the relationship between PCS and ICS can be represented as

$$\begin{cases} u = x/d_x + u_0 \\ v = y/d_y + v_0 \end{cases} \tag{3}$$

where (u, v) is the coordinate of a point in PCS, (u_0, v_0) is the pixel coordinates of the origin in ICS, d_x and d_y are the physical size of pixels. Furthermore, due to the use of an inertial sensor, a transitional coordinate system termed as 3D auxiliary coordinate system $o^{\mathrm{a}} - x^{\mathrm{a}}y^{\mathrm{a}}z^{\mathrm{a}}$ is also considered. The new coordinate system is established with the inertial sensor as the origin and is used to connect WCS to the CCS.

III. Inertial Sensor-Assisted Single View Geometry Algorithm

This section elaborates on the proposed ISA-SVG algorithm, which consists of the following three steps. First, based on the visual information captured by the image sensor, a perspective projection model is established, and the camera coordinates of the LED projection are obtained through projection transformation. Second, based on the attitude information, the transformation relationship between WCS, ACS, and CCS is established, and the attitude coordinates of the LED and LED projection are obtained through coordinate transformation. Finally, the 2D and 3D positions of the receiver are estimated based on the planar geometry theory. The detailed content of the algorithm is presented as follows.

A. Projection Transformation

Fig. 1 shows a pinhole camera. As shown in Fig. 1, the LEDs, the projection of the LEDs on the imaging plane, and the optical center lie on the same line. The PCS, ICS, and CCS of the ith LED projection are denoted as $s_i^{\mathrm{p}}\prime = (u_i^{\mathrm{p}}\prime, v_i^{\mathrm{p}}\prime)^{\mathrm{T}}\prime$, $s_i^{\mathrm{i}}\prime = \left(x_i^{\mathrm{i}}\prime, y_i^{\mathrm{i}}\prime\right)^{\mathrm{T}}\prime$ and $\mathbf{s}_i^{\mathrm{c}}\prime = (x_i^{\mathrm{c}}\prime, y_i^{\mathrm{c}}\prime, z_i^{\mathrm{c}})^{\mathrm{T}}\prime$ respectively. Based on the single-view geometry theory, the relationship between these coordinate systems is shown below

$$\begin{cases} x_i^{\mathrm{c}}\prime = x_i^{\mathrm{i}}\prime = (u_i^{\mathrm{p}}\prime - u_0)\, d_x \\ y_i^{\mathrm{c}}\prime = y_i^{\mathrm{i}}\prime = (v_i^{\mathrm{p}}\prime - v_0)\, d_y \\ z_i^{\mathrm{c}}\prime = f \end{cases} \tag{4}$$

where d_x and d_y represent the physical dimensions of each pixel in the x and y directions respectively, and the pixel coordinates of the LED can be obtained through image processing.

B. Multi-information Fusion

Since the inertial sensor cannot directly obtain the transformation relationship between the WCS and the CCS, this subsection introduces ACS to achieve the goal. First, the transformation relationship between WCS and ACS is established. Then, the transformation relationship between CCS and ACS is established. In this way, WCS and CCS are connected and the attitude information is seamlessly integrated.

The transformation relationship between WCS and ACS is shown below

$$\mathbf{s}_i^{\mathrm{a}} = \mathbf{R}_{\mathrm{w}}^{\mathrm{a}}\mathbf{s}_i^{\mathrm{w}} + \mathbf{T}_{\mathrm{w}}^{\mathrm{a}} \tag{5}$$

where $\mathbf{s}_i^{\mathrm{w}} = (x_i^{\mathrm{w}}, y_i^{\mathrm{w}}, z_i^{\mathrm{w}})^{\mathrm{T}}$ and $\mathbf{s}_i^{\mathrm{a}}=(x_i^{\mathrm{a}}, y_i^{\mathrm{a}}, z_i^{\mathrm{a}})^{\mathrm{T}}$ are the WCS and ACS coordinates of the ith LED respectively, $T_{\mathrm{w}}^{\mathrm{a}} = (t_x, t_y, t_z)^{\mathrm{T}}$ is the translation vector from WCS to ACS, and $\mathbf{R}_{\mathrm{w}}^{\mathrm{a}}$ is the rotation matrix from WCS to ACS. In particular, $\mathbf{R}_{\mathrm{w}}^{\mathrm{a}}$ can be represented in the following form

$$\mathbf{R}_{\mathrm{w}}^{\mathrm{a}} = \mathbf{R}_{X}\prime\mathbf{R}_{Y}\prime\mathbf{R}_{Z}\prime \tag{6}$$

where $\mathbf{R}_{X}\prime = \begin{bmatrix} 1 & 0 & 0 \\ 0 & \cos\alpha\prime & \sin\alpha\ \prime \\ 0 & -\sin\alpha\prime & \cos\alpha\prime \end{bmatrix}$, $\mathbf{R}_{Y}\prime = \begin{bmatrix} \cos\beta\prime & 0 & -\sin\beta\prime \\ 0 & 1 & 0 \\ \sin\beta\prime & 0 & \cos\beta\prime \end{bmatrix}$, $\mathbf{R}_{Z}\prime = \begin{bmatrix} \cos\gamma\prime & \sin\gamma\prime & 0 \\ -\sin\gamma\prime & \cos\gamma\prime & 0 \\ 0 & 0 & 1 \end{bmatrix}$, respectively, represent the rotation matrix of WCS relative to ACS in the x^w-axis, y^w-axis, and z^w-axis directions. Here, the rotation angles $\alpha\prime$, $\beta\prime$, and $\gamma\prime$ can be measured by the inertial sensor. Since the receiver's WCS and ACS are represented as $\mathbf{r}^{\mathrm{w}} = (x_r^{\mathrm{w}}, y_r^{\mathrm{w}}, z_r^{\mathrm{w}})^{\mathrm{T}}$ and $\mathbf{o}^{\mathrm{a}} = (0^{\mathrm{a}}, 0^{\mathrm{a}}, 0^{\mathrm{a}})^{\mathrm{T}}$, according to (5), we can obtain

$$r^{\mathrm{w}} = -\mathbf{R}_{\mathrm{w}}^{\mathrm{a}\ \mathrm{T}}\mathbf{T}_{\mathrm{w}}^{\mathrm{a}} \tag{7}$$

If we define $\begin{bmatrix} a_1\prime & b_1\prime & c_1\prime \\ a_2\prime & b_2\prime & c_2\prime \\ a_3\prime & b_3\prime & c_3\prime \end{bmatrix} \triangleq \mathbf{R}_{\mathrm{w}}^{\mathrm{a}}$, we have

$$\begin{aligned} \begin{bmatrix} x_r^{\mathrm{w}} \\ y_r^{\mathrm{w}} \\ z_r^{\mathrm{w}} \end{bmatrix} &= -\begin{bmatrix} a_1\prime & b_1\prime & c_1\prime \\ a_2\prime & b_2\prime & c_2\prime \\ a_3\prime & b_3\prime & c_3\prime \end{bmatrix}^{\mathrm{T}} \begin{bmatrix} t_x \\ t_y \\ t_z \end{bmatrix} \\ &= -\begin{bmatrix} a_1\prime & a_2\prime & a_3\prime \\ b_1\prime & b_2\prime & b_3\prime \\ c_1\prime & c_2\prime & c_3\prime \end{bmatrix} \begin{bmatrix} t_x \\ t_y \\ t_z \end{bmatrix} \end{aligned} \tag{8}$$

Furthermore, one can deduce that

$$t_z = -\frac{z_r^{\mathrm{w}}}{c_3\prime} - \frac{c_1\prime}{c_3\prime}t_x - \frac{c_2\prime}{c_3\prime}t_y. \tag{9}$$

Substituting (9) into (5), we have

$$\begin{cases} x_i^{\mathrm{a}} = a_1\prime x_i^{\mathrm{w}} + b_1\prime y_i^{\mathrm{w}} + c_1\prime z_i^{\mathrm{w}} + t_x \\ y_i^{\mathrm{a}} = a_2\prime x_i^{\mathrm{w}} + b_2\prime y_i^{\mathrm{w}} + c_2\prime z_i^{\mathrm{w}} + t_y \\ z_i^{\mathrm{a}} = a_3\prime x_i^{\mathrm{w}} + b_3\prime y_i^{\mathrm{w}} + c_3\prime z_i^{\mathrm{w}} - \frac{z_r^{\mathrm{w}}}{c_3\prime} - \frac{c_1\prime}{c_3\prime}t_x - \frac{c_2\prime}{c_3\prime}t_y. \end{cases} \tag{10}$$

In this way, we can determine the transformation relationship between WCS and ACS. Since the WCS of LEDs are known in advance, we can easily determine ACS of the LED according to (10). In this way, the connection between WCS and ACS is established.

Next, we further obtain the transformation relationship between CCS and ACS. Since the attitude information only

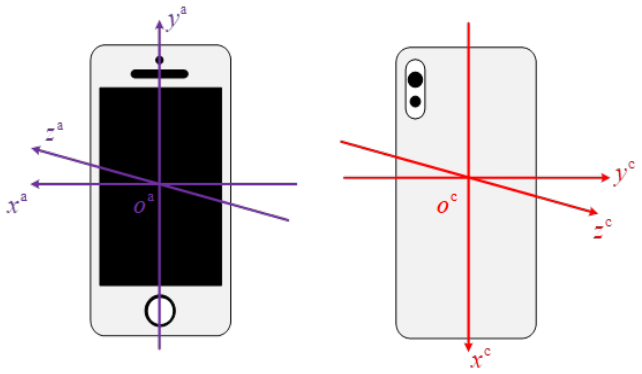

Fig. 2. The Conversion Relationship between CCS and ACS.

involves rotation transformations of the coordinates, for simplicity, we assume that the origin of CCS coincides with the origin of ACS, and only the directions of the coordinate axes are different, as shown in Fig. 2. The transformation relationship between CCS and ACS can thus be represented as

$$\begin{cases} x_i^{\mathrm{a}} = -y_i^{\mathrm{c}} \\ y_i^{\mathrm{a}} = x_i^{\mathrm{c}} \\ z_i^{\mathrm{a}} = z_i^{\mathrm{c}} \end{cases} \tag{11}$$

where $\mathbf{s}_i^{\mathrm{c}} = (x_i^{\mathrm{c}}, y_i^{\mathrm{c}}, z_i^{\mathrm{c}})^{\mathrm{T}}$ and $\mathbf{s}_i^{\mathrm{a}} = (x_i^{\mathrm{a}}, y_i^{\mathrm{a}}, z_i^{\mathrm{a}})^{\mathrm{T}}$ are respectively the CCS and ACS of the ith LED. In this way, the connection between WCS and CCS is established according to (10) and (11).

C. Position Estimation

For 2D positioning with known z_r^{w}, there are only two unknowns in (10), i.e. t_x and t_y. If we set $k_1 = -\frac{c_1\prime}{c_3\prime}$, $k_2 = -\frac{c_2\prime}{c_3\prime}$, $m_1 = a_1\prime x_i^{\mathrm{w}} + b_1\prime y_i^{\mathrm{w}} + c_1\prime z_i^{\mathrm{w}}$, $m_2 = a_2\prime x_i^{\mathrm{w}} + b_2\prime y_i^{\mathrm{w}} + c_2\prime z_i^{\mathrm{w}}$, and $m_3 = a_3\prime x_i^{\mathrm{w}} + b_3\prime y_i^{\mathrm{w}} + c_3\prime z_i^{\mathrm{w}} - \frac{z_r^{\mathrm{w}}}{c_3\prime}$, then we can simplify (10) as follows

$$\begin{cases} x_i^{\mathrm{a}}\prime = t_x + m_1 \\ y_i^{\mathrm{a}}\prime = t_y + m_2 \\ z_i^{\mathrm{a}}\prime = k_1 t_x + k_2 t_y + m_3. \end{cases} \tag{12}$$

Due to the fact that the projection of LEDs and the origin of ACS lie on the same straight line, according to the collinearity theorem, we can obtain

$$\frac{x_i^{\mathrm{a}}\prime}{x_i^{\mathrm{a}}} = \frac{y_i^{\mathrm{a}}\prime}{y_i^{\mathrm{a}}} = \frac{z_i^{\mathrm{a}}\prime}{z_i^{\mathrm{a}}}. \tag{13}$$

Substituting (11) and (12) into (13), we obtain

$$\begin{cases} (k_1 x_i^{\mathrm{a}} - f)\, t_x + k_2 x_i^{\mathrm{a}} t_y = -m_3 x_i^{\mathrm{a}} + m_1 f \\ (k_1 y_i^{\mathrm{a}} t_x + (k_2 y_i^{\mathrm{a}} - f)\, t_y = -m_3 y_i^{\mathrm{a}} + m_2 f. \end{cases} \tag{14}$$

Based on the above equation, we can obtain t_x and t_y, and then substitute them into (9) to solve for t_z. Finally, based on (8), we can estimate the position of the receiver.

$$\begin{cases} x_r^{\mathrm{w}} = -a_1\prime t_x - a_2\prime t_y - a_3\prime t_z \\ y_r^{\mathrm{w}} = -b_1\prime t_x - b_2\prime t_y - b_3\prime t_z \end{cases} \tag{15}$$

Algorithm 1 ISA-SVG Algorithm.

Input:
The Number of LED K;
World coordinates of LED $s_1^{\mathrm{w}} \sim s_K^{\mathrm{w}}$;
Pixel coordinates of LED projection $s_1^{\mathrm{p}}\prime \sim s_K^{\mathrm{p}}\prime$;

Output:
WCS of the receiver r^{w};

While $K \geq 2$ do
For $i = 1 \rightarrow K$ do
Obtain the camera coordinates s_i^{c} of the LED projection according to (4).
Obtain the orientation $\mathbf{s}_i^{\mathrm{a}}$ of the LED based on (10).
Obtain the orientation $\mathbf{s}_i^{\mathrm{a}}\prime$ of the LED projection based on (11).
End
Estimate the receiver's position $r^{\mathrm{w}}{=}(x_r^{\mathrm{w}}, y_r^{\mathrm{w}}, z_r^{\mathrm{w}})$ using planar geometry theory based on (15).
End

TABLE I
DEVICE PARAMETERS

Parameters		Model/Values
LED	Model	Addlon ADL-TD01B
	Semi-angle	$\Phi_{1/2} = 67.5^{\circ}$
	Transmitter Power	$P_t = 5$ W
	Radius	3.5 cm
Camera	Model	Rear camera of Realme Q2i
	Intrinsic parameters	$f = 3.462$ mm
		$d_u = d_v = 1.12 \times 10^{-3}$ mm
		$(u_0, v_0) = (2080, 1560)$

In conclusion, when z_r^{w} is known, ISA-SVG algorithm can achieve 2D positioning using a single LED. Note that since the position can be estimated based on linear equations, the proposed ISA-SVG is also efficient. When z_r^{w} is unknown, since (10) contains three unknowns: t_x, t_y, and z_r^{w}, and thus a single LED cannot solve for all three unknowns parameters. In this case, it is necessary to introduce another LED. In other words, the ISA-SVG algorithm can achieve 3D positioning using two LEDs. Since the computation process for 3D positioning is similar to that of 2D positioning, we will not delve into it here. Please refer to Algorithm 1 for the detailed steps of the ISA-SVG algorithm.

IV. IMPLEMENTATION OF ISA-SVG

To verify the feasibility of the proposed algorithm, we built an experimental platform. The experiment was carried out at the space of 120 cm × 120 cm × 240 cm, with three LEDs installed on the ceiling at coordinates of $[24.2, 32.3, 240]^{\mathrm{T}}$, $[94.9, 32.2, 240]^{\mathrm{T}}$, and $[95.2, 101.9, 240]^{\mathrm{T}}$ (in centimeters). The experimental platform is shown in Fig. 3 and the system specifications are given in Table I.

At the transmitter side, commercial high-power LEDs are used as transmitters to provide both illumination and location landmarks, which is in line with practical scenarios. A personal computer is used for data preprocessing, encompassing data frame structuring and encoding procedures. To ensure packet synchronization, the data frame comprises a Start Frame

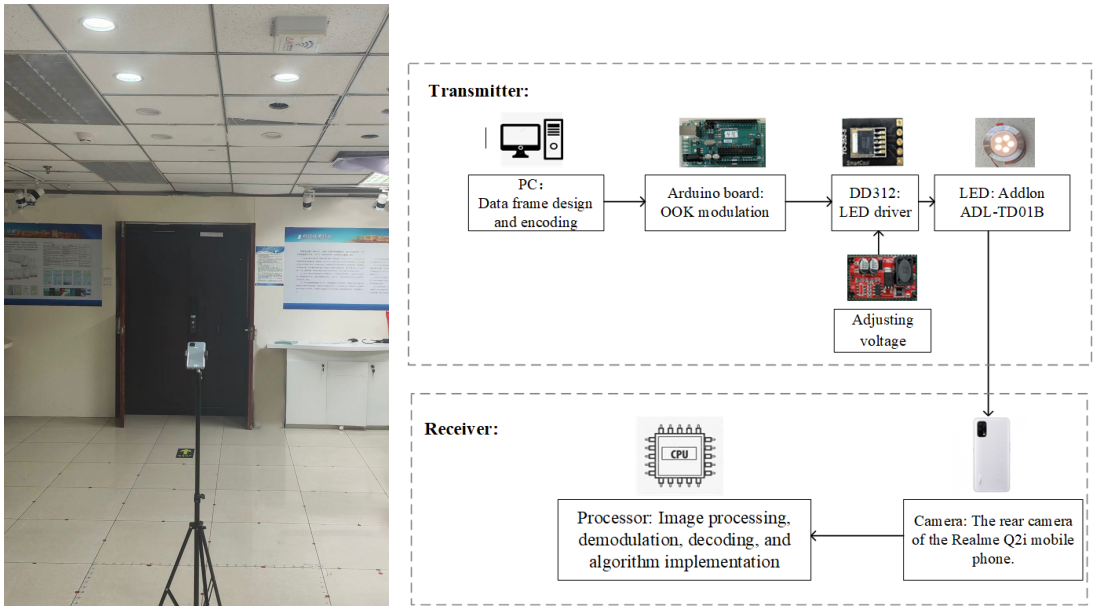

(a) Test-bed environment (b) Block diagram

Fig. 3. Experimental setup.

Delimiter (SFD) and identity information, with SFD being constituted by single-byte data and Barker codes. Furthermore, Manchester encoding is used to mitigate flickering concerns, while an Arduino development board is utilized for On-off Keying (OOK) modulation, a voltage up-down board for voltage regulation, and a DD312 chip for drive current generation. Ultimately, the transmitter's identity information is disseminated via LED broadcast.

At the receiver, the receiver utilizes a commercial Android smartphone, the Realme Q2i 5G model, with its camera serving as the image sensor. The pixel coordinates of the principal point are $(u_0^{\mathrm{p}}, v_0^{\mathrm{p}})= (2080, 1560)$, the physical size of the pixels is $d_x = d_y = 1.12\ \mu\mathrm{m}$, the focal length is $f = 3.462\ \mathrm{mm}$, and the exposure time and frame rate are 0.125 ms and 30 fps, respectively. The phone's built-in accelerometer, gyroscope, and magnetometer serve as inertial sensors. The data measured by the accelerometer and magnetometer can be used to calculate the phone's three rotation angles. Android has encapsulated the calculation process into dedicated application programming interfaces for direct user access. The entire positioning process at the receiver end involves image processing, demodulation, decoding, and algorithm implementation, all of which are completed by the smartphone's processor. Note that due to the projection principle of cameras, the camera can project different LEDs on the different areas of the image plane, and thus it can filter out the interference light and extra LEDs useless for positioning. That means ISA-SVG is robust to environment variation. The experiment results will be shown in the next section.

V. Simulation and Experimental Results

This section evaluates the performance of ISA-SVG via both simulation and experimental results.

A. Simulation Results

In the simulation, a scenario with four LEDs is considered with the coordinates of the LEDs being (3.5,3.5,3), (3.5,4.5,3), (4.5,3.5,3), and (4.5,4.5,3) (in meters), and a half-power angle of 60 degrees. The indoor space has dimensions of 8 m × 6 m × 3 m. The sampling points of the receiver have a discrete step size of 10 cm along each coordinate axis, resulting in a total of 80 × 60 × 30 = 144000 positioning points for simulation. The coverage ratio (CR) is used to evaluate the coverage performance of a positioning algorithm, which is defined as:

$$CR = \frac{N_{\text{effective}}}{N_{\text{total}}} \times 100\% \tag{16}$$

where $N_{\text{effective}}$ represents the number of positions where the receiver can detect a sufficient number of LEDs for positioning, N_{total} represents the total number of measured positions.

As shown in Fig. 4, to verify the coverage performance, we conduct three fused VLP algorithms, including ISA-SVG, an inertial measurement unit-based single LED VLP algorithm (V-IMU) [16] and a camera-assisted received signal strength (CA-RSS) algorithm [18]. The receiver's field of view angle ranges from 0° to 80°, and the receiver orientation is considered arbitrarily. It can be observed that the coverage ratios of ISA-SVG and V-IMU rapidly increase from 0 to 95%, and they have better coverage performance than that of CA-RSS. This is because both ISA-SVG and V-IMU require only a single LED for 2D positioning, while CA-RSS requires three LEDs. With the assistance of the IMU, the ISA-SVG algorithm is not limited by the receiver orientation, allowing it to achieve a high coverage ratio with reliable positioning accuracy.

Fig. 5 further illustrates the cumulative distribution function (CDF) curves of the proposed ISA-SVG and the two baseline

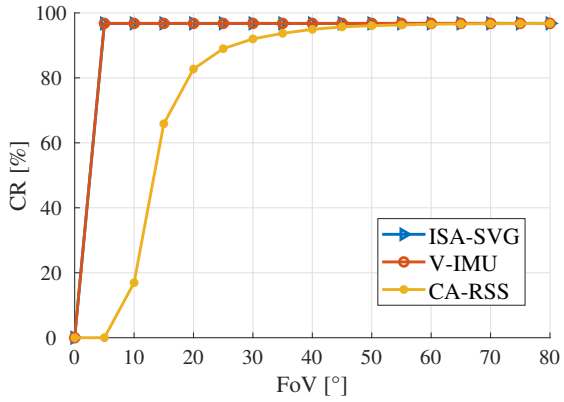

Fig. 4. The comparison of coverage ratios for positioning among ISA-SVG, V-IMU, and CA-RSS algorithms with arbitrary receiver orientations.

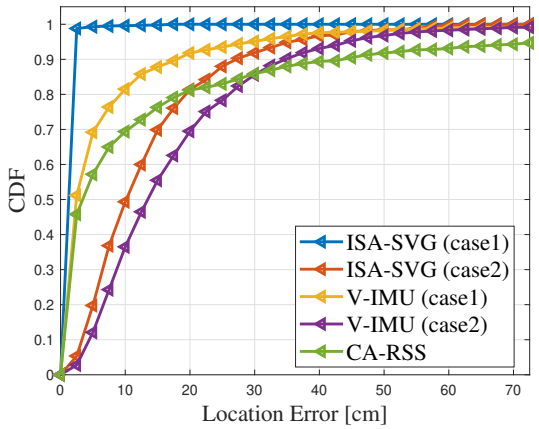

Fig. 5. The 2D positioning accuracy performance of ISA-SVG, V-IMU, and CA-RSS algorithms.

algorithms. Since both ISA-SVG and V-IMU require IMU to obtain rotation angles, we consider two cases. In case 1, we consider the ideal case with no measurement error, while in the second case, we impose random measurement errors uniformly distributed in $[-1.5°, 1.5°]$ on the pitch and roll angles and random measurement errors uniformly distributed in $[-5°, 5°]$ on the yaw angle [19]. It can be observed that the proposed ISA-SVG can always achieve the best performance in case 1. Moreover, ISA-SVG can also outperform the baseline scheme in case 2 with IMU measurement deviations. That means the proposed ISA-SVG is also robust to the imperfections of the hardware, which will further be validated in the experimental results in the next subsection.

B. Experiment Results

This subsection presents the experimental results of the ISA-SVG algorithm. First, the 2D positioning accuracy of the ISA-SVG algorithm under different receiver orientations is evaluated. As shown in Fig. 6, when the receiver is horizontal, the minimum error, maximum error, and average error of the positioning results are 1.78 cm, 6.57 cm, and 4.68 cm respectively. When the receiver rotates 30° around the x-axis, the minimum error, maximum error, and average error of the positioning results are 2.57 cm, 10.64 cm, and 5.74 cm. When the receiver rotates 30° around the y-axis, the minimum error, maximum error, and average error of the positioning results are 2.83 cm, 11.75 cm, and 6.03 cm. It can be observed that under different receiver orientations, the positioning errors of the ISA-SVG algorithm are constantly within 12 cm, validating the effectiveness and stability of the proposed algorithm in practical applications.

Furthermore, the 3D positioning accuracy of the ISA-SVG algorithm under different receiver orientations is further evaluated. As shown in Fig. 7, when the receiver is horizontal, the minimum error, maximum error, and average error of the positioning results are 2.22 cm, 9.38 cm, and 5.63 cm respectively. When the receiver rotates 30° around x-axis, the minimum error, maximum error, and average error of the positioning results are 3.47 cm, 11.32 cm, and 6.01 cm. When the receiver rotates 30° around the y-axis, the minimum error, maximum error, and average error of the positioning results are 4.27 cm, 12.69 cm, and 6.79 cm. It can be seen that compared to 2D positioning, the error in 3D positioning only slightly increases but still remains at a relatively low level. Therefore, the ISA-SVG algorithm can achieve high-precision positioning while ensuring high coverage.

The 2D and 3D positioning accuracy of the ISA-SVG algorithm in a mobile environment is also evaluated. In this experiment, the receiver moved along a rectangular path. The positioning results in a mobile environment were repeatedly measured and then summarized. As shown in Fig. 8, the overall trend of the positioning results closely matched the actual path. For 2D positioning, the maximum, minimum, and average positioning accuracy are 11.33 cm, 2.53 cm, and 5.04 cm, respectively. Besides, the maximum, minimum, and average 3D positioning accuracy are 12.65 cm, 3.02 cm, and 6.31 cm, respectively. Therefore, the deviation errors between estimated coordinates and the actual path in a mobile environment were all within 13 cm. The experimental results verify that the proposed ISA-SVG algorithm can achieve stable performance in the mobile environment.

To further expand the considered scenarios, Fig. 9 evaluates the positioning accuracy of ISA-SVG with different heights and orientations. It can be observed that ISA-SVG achieves stable performance under different heights and tilted angles. For instance, when the height of the receiver is 90 cm with 0-degree titled angle, more than 98% samples can achieve an accuracy of 10 cm. With the height and tilted angle increasing, the positioning accuracy decreases slightly but still achieve fair good performance. For instance, when the height of the receiver is 120 cm with 30-degree titled angle, about 88% samples can still achieve accuracy within 10 cm.

VI. Conclusion

In this paper, we propose an inertial sensor-assisted single-view geometry algorithm to address the coverage limitation issue of traditional visible light positioning algorithms and achieve accurate positioning with as little as one LED. Particularly, we first establish a pose fusion model that effectively

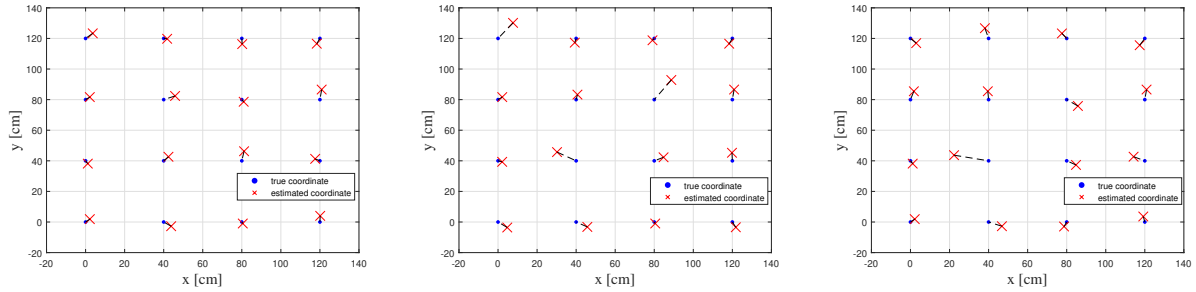

(a) the receiver is horizontal. (b) the receiver rotates 30° around the x-axis. (c) the receiver rotates 30° around the y-axis.

Fig. 6. The 2D positioning accuracy of the ISA-SVG algorithm under different receiver orientations.

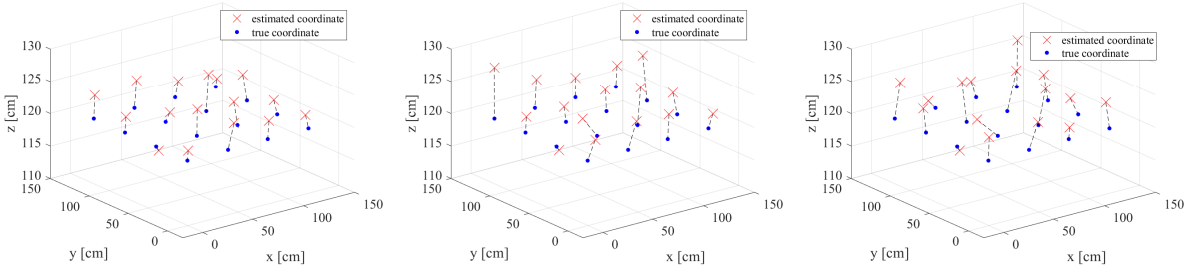

(a) the receiver is horizontal. (b) the receiver rotates 30° around the X-axis. (c) the receiver rotates 30° around the y-axis.

Fig. 7. The 3D positioning accuracy of the ISA-SVG ccalgorithm under different receiver orientations.

fuses the inertial sensor information and VLP information. Based on single-view geometry theory, the ISA-SVG algorithm obtains the camera coordinates of LED projection. Then, by introducing an orientation coordinate system, it establishes a link between WCS and CCS to further derive the orientation coordinates of LED and LED projection. Finally, the receiver's position is estimated based on planar geometry theory. The ISA-SVG algorithm enables 2D positioning of a single LED and 3D positioning of dual LEDs. Simulation results show that the coverage rate of the ISA-SVG algorithm is over 95%. Experimental results show that the proposed method can achieve an average positioning error as low as 4.70 cm. In future, it is interesting to further expand this work to outdoor scenarios.

REFERENCES

[1] P. S. Farahsari, A. Farahzadi, J. Rezazadeh, and A. Bagheri, "A survey on indoor positioning systems for IoT-based applications," *IEEE Internet of Things Journal*, vol. 9, no. 10, pp. 7680–7699, 2022.

[2] L. Oostwegel, "Indoor positioning using augmented reality," 2020.

[3] E. Díaz, M. C. Pérez, D. Gualda, J. M. Villadangos, J. Ureña, and J. J. García, "Ultrasonic indoor positioning for smart environments: A mobile application," in *2017 4th Experiment@International Conference (exp.at'17)*, 2017, pp. 280–285.

[4] P. Dabove, V. Di Pietra, M. Piras, A. A. Jabbar, and S. A. Kazim, "Indoor positioning using ultra-wide band UWB technologies: Positioning accuracies and sensors' performances," in *2018 IEEE/ION Position, Location and Navigation Symposium (PLANS)*. IEEE, 2018, pp. 175–184.

[5] S. Shang and L. Wang, "Overview of WiFi fingerprinting-based indoor positioning," *IET Communications*, vol. 16, no. 7, pp. 725–733, 2022.

[6] L. Bai, F. Ciravegna, R. Bond, and M. Mulvenna, "A low cost indoor positioning system using bluetooth low energy," *Ieee Access*, vol. 8, pp. 136 858–136 871, 2020.

[7] Z. Zhu, Y. Yang, M. Chen, C. Guo, J. Cheng, and S. Cui, "A survey on indoor visible light positioning systems: Fundamentals, applications, and challenges," *arXiv preprint arXiv:2401.13893*, 2024.

[8] S. Bastiaens, M. Alijani, W. Joseph, and D. Plets, "Visible light positioning as a next-generation indoor positioning technology: A tutorial," *IEEE Communications Surveys & Tutorials*, 2024.

[9] A. H. A. Bakar, T. Glass, H. Y. Tee, F. Alam, and M. Legg, "Accurate visible light positioning using multiple-photodiode receiver and machine learning," *IEEE Transactions on Instrumentation and Measurement*, vol. 70, pp. 1–12, 2020.

[10] B. Hussain, Y. Wang, R. Chen, and C. P. Yue, "Camera pose estimation using a VLC-modulated single rectangular LED for indoor positioning," *IEEE Transactions on instrumentation and measurement*, vol. 71, pp. 1–11, 2022.

[11] X. Guo, N. Ansari, F. Hu, Y. Shao, N. R. Elikplim, and L. Li, "A survey on fusion-based indoor positioning," *IEEE Communications Surveys & Tutorials*, vol. 22, no. 1, pp. 566–594, 2019.

[12] S. H. Oh and J. G. Kim, "Vlc positioning by dnn via wknn in indoor environment," in *2022 Thirteenth International Conference on Ubiquitous and Future Networks (ICUFN)*, 2022, pp. 450–453.

[13] S. Shen, S. Li, and H. Steendam, "Hybrid position and orientation estimation for visible light systems in the presence of prior information on the orientation," *IEEE Transactions on Wireless Communications*, vol. 21, no. 8, pp. 6271–6284, 2022.

[14] R. Zhang, W.-D. Zhong, D. Wu, and K. Qian, "A novel sensor fusion based indoor visible light positioning system," in *2016 IEEE globecom workshops (GC wkshps)*. IEEE, 2016, pp. 1–6.

[15] Y. Wang, B. Hussain, and C. P. Yue, "Arbitrarily tilted receiver camera correction and partially blocked LED image compensation for indoor visible light positioning," *IEEE Sensors Journal*, vol. 22, no. 6, pp. 4800–4807, 2021.

[16] H. Cheng, C. Xiao, Y. Ji, J. Ni, and T. Wang, "A single LED visible light positioning system based on geometric features and CMOS camera," *IEEE Photonics Technology Letters*, vol. 32, no. 17, pp. 1097–1100, 2020.

[17] S. Wen, Z. Ge, D. Yuan, Y. Chen, F. Wen, J. Xu, and W. Guan, "Enhanced pedestrian navigation on smartphones with vlp-assisted pdr integration," *IEEE Sensors Journal*, 2023.

[18] Y. Yang, C. Li, R. Bao, C. Guo, C. Feng, and J. Cheng, "Multi-angle camera assisted received signal strength algorithm for visible

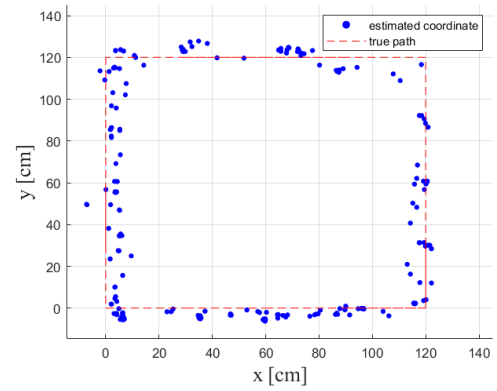

(a) 2D positioning

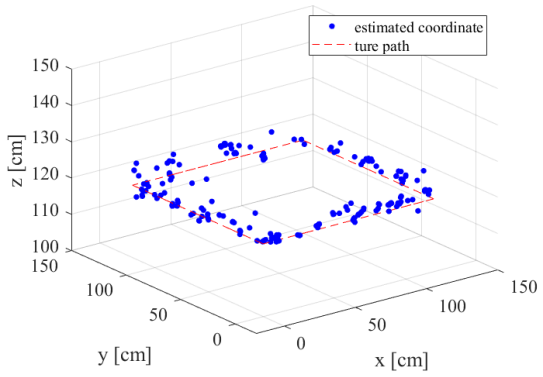

(b) 3D positioning

Fig. 8. Localization accuracy of the ISA-SVG algorithm in a mobile environment.

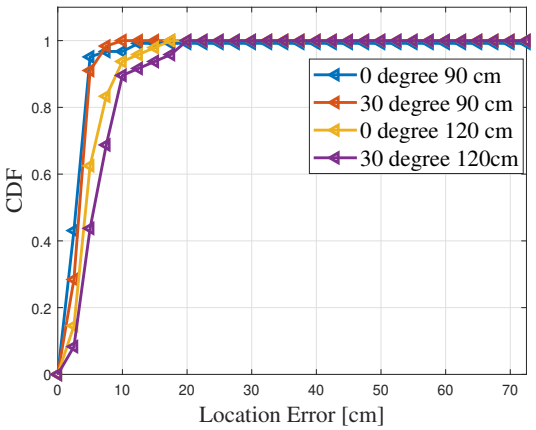

Fig. 9. The positioning performance of ISA-SVG with different heights and orientations.

light positioning," *Journal of Lightwave Technology*, vol. 39, no. 23, pp. 7435–7446, 2021.

[19] J. Hao, J. Chen, and R. Wang, "Visible light positioning using a single led luminaire," *IEEE Photonics Journal*, vol. 11, no. 5, pp. 1–13, 2019.